Stellate multiform amelanotic choroidopathy: clinical and multimodal imaging features

Ramtohul, P.; Pellegrini, M.; Pichi, F.; Preziosa, C.; Marchese, A.; Cicinelli, M.V.; ... ; Freund, K.B.

STELLATE MULTIFORM AMELANOTIC CHOROIDOPATHY

Clinical and Multimodal Imaging Features

PRITHVI RAMTOHUL, MD,* MARCO PELLEGRINI, MD,† FRANCESCO PICHI, MD,‡ CHIARA PREZIOSA, MD,† ALESSANDRO MARCHESE, MD,§¶ MARIA VITTORIA CICINELLI, MD,¶** ELISABETTA MISEROCCHI, MD,¶** RUSDEEP MUNDAE, MD,* SARAH MREJEN, MD,†† SORAYA ROFAGHA, MD,‡‡§§ CALVIN E. MEIN, MD,¶¶ LUKE MEIN, MD,¶¶ MICHAEL D. OBER, MD,*** EDUARDO CUNHA DE SOUZA, MD,††† SALOMON YVES COHEN, MD PHD,¶ ELON H. C. VAN DIJK, MD, PHD,‡‡‡ LEE JAMPOL, MD,§ CAMIEL J. F. BOON, MD, PHD,‡‡‡§§§ K. BAILEY FREUND, MD*¶¶¶

Purpose: To describe the clinical and multimodal imaging features of stellate multiform amelanotic choroidopathy (SMACH; also known as serous maculopathy due to aspecific choroidopathy).

Methods: Retrospective observational case series of eyes presenting with SMACH. Multimodal imaging including fundus photography, optical coherence tomography (OCT), OCT angiography (OCTA), and indocyanine green angiography (ICGA) was analyzed.

Results: Eighteen eyes from 18 patients (mean age: 28 ± 19 years) were included. The mean follow-up duration was 9 years. Ophthalmoscopy showed a yellowish orange, dendriform choroidal lesion. At presentation, subretinal fluid (SRF) was seen in 10 of 18 cases (56%). Eight patients (44%) showed no evidence of SRF during a mean follow-up of 6 years. Cross-sectional OCT showed hyperreflective fibrous-like changes within the inner choroid with choriocapillaris flow preservation on OCTA. En face OCT showed a hyperreflective choroidal lesion with finger-like projections oriented in a stellate configuration. On ICGA, SMACH showed early and late hypofluorescence. None of the cases showed lesion growth.

Conclusion: SMACH seems to be a unilateral choroidopathy characterized by distinctive multimodal imaging features. As SRF was absent in some cases, while a dendriform pattern was a consistent finding in all eyes, the authors propose renaming this entity "stellate multiform amelanotic choroidopathy," a name that retains its previous abbreviation "SMACH."

RETINA 43:1448–1461, 2023

Serous maculopathy due to aspecific choroidopathy (SMACH) is a newly described and uncommon macular disorder first reported in a young patient by Van Dijk and Boon in 2021.[1] To our knowledge, only two additional cases have been described since.[2] Clinically, SMACH is characterized by subretinal fluid (SRF) accumulation overlying areas of retinal pigment epithelium (RPE) changes. Adjunctive multimodal imaging features including fundus autofluorescence imaging (FAF) and fluorescein angiography (FA) show nonspecific findings related to outer retinal and RPE alterations.[1] Optical coherence tomography (OCT) is the most relevant imaging modality for the diagnosis of SMACH and shows SRF with an irregular and thickened RPE elevated by an underlying thickened choroid.[1] Importantly, a structurally altered and hyperreflective choroid on OCT seems to be the key feature of SMACH.[1] Nonetheless, a certain degree of overlap may exist with conditions associated with SRF in young patients, such as central serous chorioretinopathy (CSC), Best vitelliform macular dystrophy, inflammatory chorioretinopathies, or choroidal tumors. Because limited descriptions of SMACH exist in the literature, there is a need to expand the clinical and multimodal imaging characterization of this entity.

The purpose of this study was to describe the clinical features, multimodal imaging findings, treatment responses, and long-term course of SMACH.

Methods

This is an observational, retrospective, multicenter case series of patients presenting with clinical and multimodal imaging findings compatible with the original description of SMACH.[1] Each coauthor identified cases of SMACH through the use of patient lists, keywords, or diagnostic indicators applied to their database from 2006 to 2022. This study was approved by the Western Institutional Review Board (Olympia, WA), and written informed consent was not required because of the retrospective nature of this study. This report adhered to the tenets of the Declaration of Helsinki and complied with the Health Insurance Portability and Accountability Act.

The inclusion criteria were eyes with findings on multimodal imaging consistent with SMACH, defined as serous retinal detachment associated with pigmentary changes on ophthalmoscopy, disruption and elevation of the RPE by a thickened and structurally altered choroid on OCT, hypofluorescent and hyperfluorescent changes on FA, absence of focal choroidal hyperpermeability on indocyanine green angiography (ICGA), and absence of macular neovascularization (MNV) on OCT angiography (OCTA).[1] Extramacular lesions or eyes without serous retinal detachment but showing a similar imaging pattern were also included.

All patients underwent a complete ophthalmologic examination, including measurement of the best-corrected visual acuity (BCVA) using Snellen charts, slit-lamp biomicroscopy, and indirect fundus ophthalmoscopy. Color fundus photographs (EIDON AF, Centervue Padova, Italy; Topcon TRC-50IX retinal camera, Topcon Medical Systems, Oakland, NJ; or Clarus 500, Carl Zeiss Meditec AG), spectral-domain OCT (SD-OCT; Spectralis, Heidelberg Engineering, Heidelberg, Germany), high-resolution SD-OCT prototype (High-Res OCT; Heidelberg Engineering, Heidelberg, Germany), swept-source OCT (PLEX Elite 9000; Carl Zeiss Meditec, Inc, Dublin, CA), SD-OCTA (CIRRUS 6000; Carl Zeiss Meditec, Inc, Dublin, CA); and swept-source OCTA (PLEX Elite 9000; Carl Zeiss Meditec, Inc, Dublin, CA), near-infrared reflectance imaging (NIR, Spectralis, Heidelberg Engineering, Heidelberg, Germany), FAF (Spectralis HRA; Heidelberg Engineering, Heidelberg, Germany or Optos, plc), and FA and ICGA (Spectralis HRA; Heidelberg Engineering, Heidelberg, Germany) were reviewed when available. Full-field electroretinography (ERG), electro-oculography (EOG), and microperimetry (microperimetry MP-3; Nidek, Japan) were performed in selected cases. Genetic panel testing for inherited retinal diseases was collected when available.

Detailed chart reviews were performed and deidentified demographic and clinical data, including ages, genders, presenting symptoms, provisional diagnosis, ocular and systemic medical history, laboratory investigations, ocular therapies, and baseline and final Snellen BCVA were collected and summarized.

Quantitative and qualitative data are presented as mean ± SD and absolute and relative proportions, respectively.

Results

Demographic Data

Eighteen eyes from 18 patients (ten men and eight women) were included. At presentation, the mean age was 28 ± 19 years (range, 7–68 years), and the mean BCVA was 20/25 (range, 20/200–20/20). The mean follow-up duration was 9 years (range, 1–43 years), and the mean BCVA was stable at the final follow-up visit (20/25; range, 20/200–20/20). Three eyes had BCVA <20/40 at the final follow-up visit.

Presenting symptoms included gradual vision loss in seven patients, metamorphopsia in six patients, whereas seven patients were asymptomatic. At presentation, the

From the *Vitreous Retina Macula Consultants of New York, New York, New York; †Department of Biomedical and Clinical Science "Luigi Sacco," Eye Clinic, Luigi Sacco Hospital, University of Milan, Milan, Italy; ‡Eye Institute, Cleveland Clinic Abu Dhabi, Al Maryah Island, Abu Dhabi, United Arab Emirates. Cleveland Clinic Lerner College of Medicine, Case Western Reserve University, Cleveland, Ohio; §Department of Ophthalmology, Feinberg School of Medicine, Northwestern University, Chicago, Illinois; ¶Department of Ophthalmology, IRCCS San Raffaele Scientific Institute, Milan, Italy; **School of Medicine, Vita-Salute San Raffaele University, Milan, Italy; ††Ophthalmic Center for Imaging and Laser, Paris, France; ‡‡East Bay Retina Consultants, Inc, Oakland, California; §§Department of Ophthalmology, University of California, San Francisco, San Francisco, California; ¶¶Retinal Consultants of San Antonio, San Antonio, Texas; ***Department of Ophthalmology, Henry Ford Health Systems, Detroit, Michigan; †††Department of Ophthalmology, University of São Paulo (USP), São Paulo, Brazil; ‡‡‡Department of Ophthalmology, Leiden University Medical Center, Leiden, the Netherlands; §§§Department of Ophthalmology, Amsterdam University Medical Centers, Amsterdam, the Netherlands; and ¶¶¶Department of Ophthalmology, NYU Grossman School of Medicine, New York, New York

This work was supported by The Macula Foundation Inc., New York, New York. P. Ramtohul was supported by The Philippe Foundation.

None of the authors has any financial/conflicting interests to disclose.

K. B. Freund is a consultant for Heidelberg Engineering, Zeiss, Allergan, Bayer, Genentech, and Novartis and receives research support from Genentech/Roche. S. -Y. Cohen is a consultant for Allergan-Abbvie, Bayer, Novartis, Roche, and Thea. The other authors report no disclosures.

Reprint requests: K. Bailey Freund, MD, Vitreous Retina Macula Consultants of New York, 950 Third Avenue, New York, NY 10022; e-mail: kbfreund@gmail.com

suspected diagnoses included chronic CSC in four patients, placoid chorioretinitis in two patients, Best vitelliform macular dystrophy in one patient, inherited retinal dystrophy in one patient, torpedo maculopathy in one patient, choroidal osteoma in one patient, choroidal nodule in one patient, choroidal metastasis in one patient, amelanotic choroidal nevus in one patient, choroidal hemangioma in one patient, unspecified maculopathy in two patients, and unspecified choroidal tumor in two patients. Ocular and systemic medical history was unremarkable in all cases. Previoius ocular treatments included photodynamic therapy (PDT, four patients with persistent SRF >6 months) and intravitreal injection of anti–vascular endothelial growth factor (anti-VEGF, three patients with persistent SRF >6 months), which all had no effect on BCVA. Laboratory

Table 1. Patient Demographics and Clinical Features

Unpublished Cases	Eye	Suspected Diagnoses at Presentation	Age at Presentation (Years)	Follow-up Duration (Years)	Sex	Presenting Symptoms	Baseline BCVA	Final BCVA	Treatments
1	OD	CSC	13	14	F	Gradual vision loss	20/25	20/50	None
2	OD	CSC	19	9	M	Gradual vision loss Metamorphopsia	20/20	20/200	PDT
3	OS	CSC	20	43	M	Gradual vision loss Metamorphopsia	20/50	20/40	None
4	OS	Placoid chorioretinitis	9	3	F	Asymptomatic	20/20	20/20	None
5	OS	Placoid chorioretinitis	15	2	M	Asymptomatic	20/20	20/20	None
6	OS	Best disease	7	13	M	Gradual vision loss	20/32	20/20	PDT Anti-VEGF IVI
7	OD	Inherited retinal dystrophy	17	2	F	Asymptomatic	20/20	20/20	None
8	OS	Torpedo maculopathy	15	6	M	Asymptomatic	20/20	20/20	None
9	OS	Choroidal osteoma	45	6	F	Metamorphopsia	20/25	20/25	None
10	OS	Choroidal nodule	40	8	F	Asymptomatic	20/20	20/20	None
11	OD	Choroidal metastasis	51	1	F	Gradual vision loss	20/25	20/20	None
12	OD	Choroidal nevus	29	19	M	Asymptomatic	20/20	20/20	None
13	OD	Unspecified maculopathy	27	4	F	Gradual vision loss	20/30	20/30	None
14	OD	Unspecified maculopathy	68	6	F	Gradual vision loss	20/25	20/25	None
15	OS	Unspecified choroidal tumor	51	6	M	Asymptomatic	20/20	20/20	None

Previously Published Cases[1,2]	Eye	Suspected Diagnoses at Presentation	Age at Presentation (Years)	Follow-up Duration (Years)	Sex	Presenting Symptoms	Baseline BCVA	Final BCVA	Treatments
1	OS	Choroidal hemangioma	18	3	M	Metamorphopsia	20/20	20/20	PDT Anti-VEGF IVI
2	OS	Choroidal tumor	35	1	M	Metamorphopsia	20/25	20/32	PDT Anti-VEGF
3	OS	CSC	30	7	M	Metamorphopsia	20/20	20/20	None

BCVA, best-corrected visual acuity; CSC, central serous chorioretinopathy; F, female; IVI, intravitreal injection; M, male; OD, right eye; OS, left eye; PDT, photodynamic therapy, VEGF: vascular endothelial growth factor.

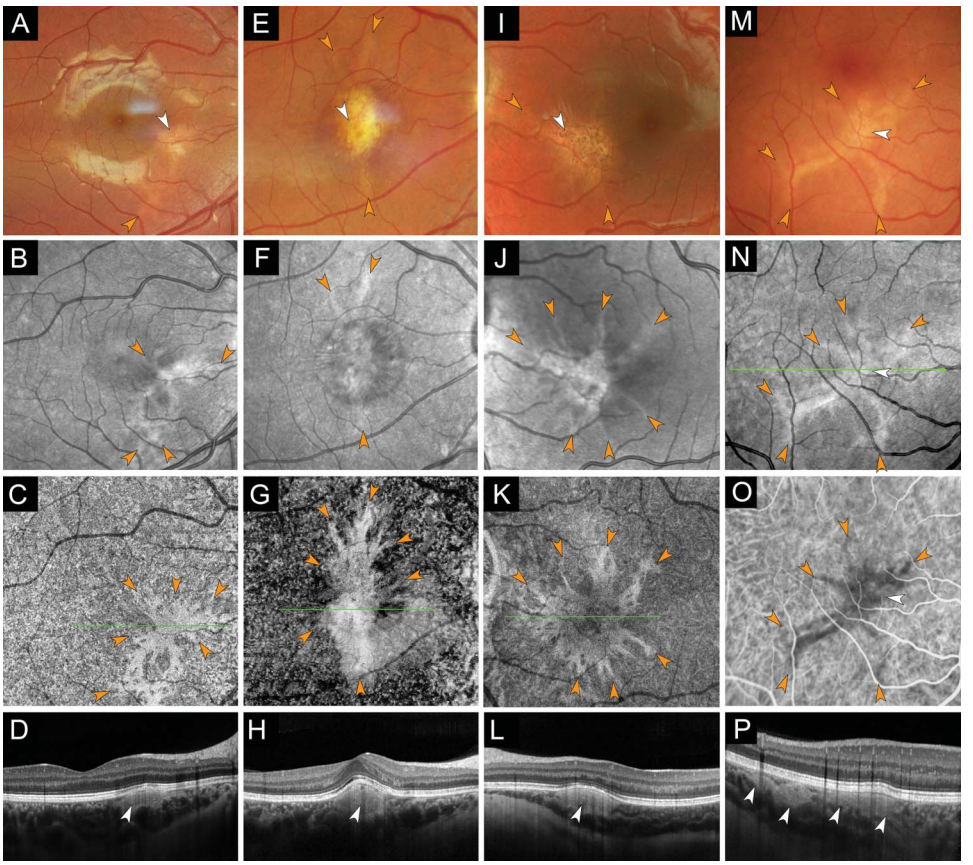

Fig. 1. Representative cases of stellate multiform amelanotic choroidopathy (SMACH) without subretinal fluid on multimodal imaging. **A–D.** Case 7. Patient diagnosed with inherited retinal dystrophy at the age of 17 years. **A.** Pseudocolor fundus photography of the right eye shows a parafoveal, yellowish orange, dendriform, choroidal lesion (*white arrowhead*). Note the distinctive finger-like projection pointing inferiorly (*orange arrowhead*). **B.** On the near-infrared reflectance image, the lesion is hyperreflective (*white arrowhead*) with distinctive hyperreflective finger-like projections pointing radially (*orange arrowheads*). **C.** En face structural optical coherence tomography (OCT) segmented at the level of the choroidal lesion shows hyperreflective changes with distinctive hyperreflective finger-like projections (*orange arrowheads*) more numerous than seen on ophthalmoscopy. The extent of the choroidal lesion on en face structural OCT exceeds the one assessed on ophthalmoscopy. The green line indicates the location of the OCT B-scan in (**D**). **D.** Spectral-domain OCT B-scan shows hyperreflective fibrous-like changes of the inner choroid (*white arrowhead*) resulting in mild anterior protrusion and alteration of the retinal pigment epithelium (RPE). Note the relative preservation of the overlying ellipsoid and interdigitation zones and the absence of subretinal fluid. The normal outer choroidal vasculature beneath the choroidal lesion is visible. **E–H.** Case 11. Patient diagnosed with choroidal metastasis at the age of 51 years. **E.** Pseudocolor fundus photography of the right eye shows a subfoveal, yellowish orange, dendriform, choroidal lesion with overlying hypopigmentary changes (*white arrowhead*). Note the distinctive finger-like projections pointing superiorly and inferiorly (*orange arrowheads*). **F.** On the near-infrared reflectance image, the lesion is hyperreflective (*white arrowhead*) with distinctive hyperreflective finger-like projections pointing superiorly and inferiorly (*orange arrowheads*). **G.** En face structural OCT segmented at the level of the choroidal lesion shows hyperreflective changes with distinctive hyperreflective finger-like projections (*orange arrowheads*) more numerous than seen on ophthalmoscopy. The extent of the choroidal lesion on en face structural OCT exceeds the one assessed on ophthalmoscopy. The green line indicates the location of the OCT B-scan in (**H**). **H.** Spectral-domain OCT B-scan shows hyperreflective fibrous-like changes of the inner choroid (*white arrowhead*), resulting in anterior protrusion and alteration of the RPE. Note the relative preservation of the overlying ellipsoid and interdigitation zones and the absence of subretinal fluid. The normal outer choroidal vasculature beneath the choroidal lesion is visible. **I–L.** Case 4. Patient diagnosed with placoid chorioretinitis at the age of 9 years. **I.** Pseudocolor fundus photography of the left eye shows a parafoveal, yellowish orange, dendriform, choroidal lesion with overlying hypopigmentary and hyperpigmentary changes (*white arrowhead*). Note the distinctive finger-like projections pointing superiorly and inferiorly (*orange arrowheads*). **J.** On the near-infrared reflectance image, the lesion is hyperreflective (*white arrowhead*) with distinctive hyperreflective finger-like projections pointing radially in a stellate configuration (*orange arrowheads*). **K.** En face structural OCT segmented at the level of the choroidal lesion shows hyperreflective changes with distinctive hyperreflective finger-like projections (*orange arrowheads*) more numerous than seen on ophthalmoscopy. The extent of the choroidal lesion on en face structural OCT exceeds the one assessed on ophthalmoscopy. The green line indicates the location of the OCT B-scan in (**L**). **L.** Spectral-domain OCT B-scan shows hyperreflective fibrous-like changes of the inner choroid (*white arrowhead*), resulting in anterior protrusion and alteration of the RPE. Note the focal attenuation of the overlying ellipsoid and interdigitation zones and the absence of subretinal fluid. The normal outer choroidal vasculature beneath the choroidal lesion is visible. **M–P.** Case 12. Patient diagnosed with amelanotic choroidal nevus at the age of 29 years. **M.** Pseudocolor fundus photography of the right eye shows a parafoveal, yellowish orange, dendriform, choroidal lesion (*white arrowhead*). Note the distinctive finger-like projections pointing radially in a stellate configuration (*orange arrowheads*). **N.** On the near-infrared reflectance image, the lesion is hyperreflective (*white arrowhead*) with distinctive hyperreflective finger-like projections pointing radially in a stellate configuration (*orange arrowheads*). The green line indicates the location of the OCT B-scan in (**P**). **O.** Early phase of indocyanine green angiography shows a hypofluorescent choroidal lesion (*white arrowhead*) with distinctive hypofluorescent finger-like projections arranged in a stellate configuration (*orange arrowheads*). **P.** Spectral-domain OCT B-scan shows hyperreflective fibrous-like changes of the inner choroid (*white arrowheads*), resulting in mild anterior protrusion and alteration of the RPE. Note the relative preservation of the overlying ellipsoid and interdigitation zones and the absence of subretinal fluid. The normal outer choroidal vasculature beneath the choroidal lesion is visible.

work-up including complete blood count and infectious disease serologies (tuberculosis, Lyme disease, toxoplasmosis, rubella, and cytomegalovirus) was performed in 3 cases and was unremarkable. Panel-based genetic testing for inherited retinal diseases was performed in 4 cases, and no pathogenic mutations were found. Table 1 summarizes the demographic and clinical findings.

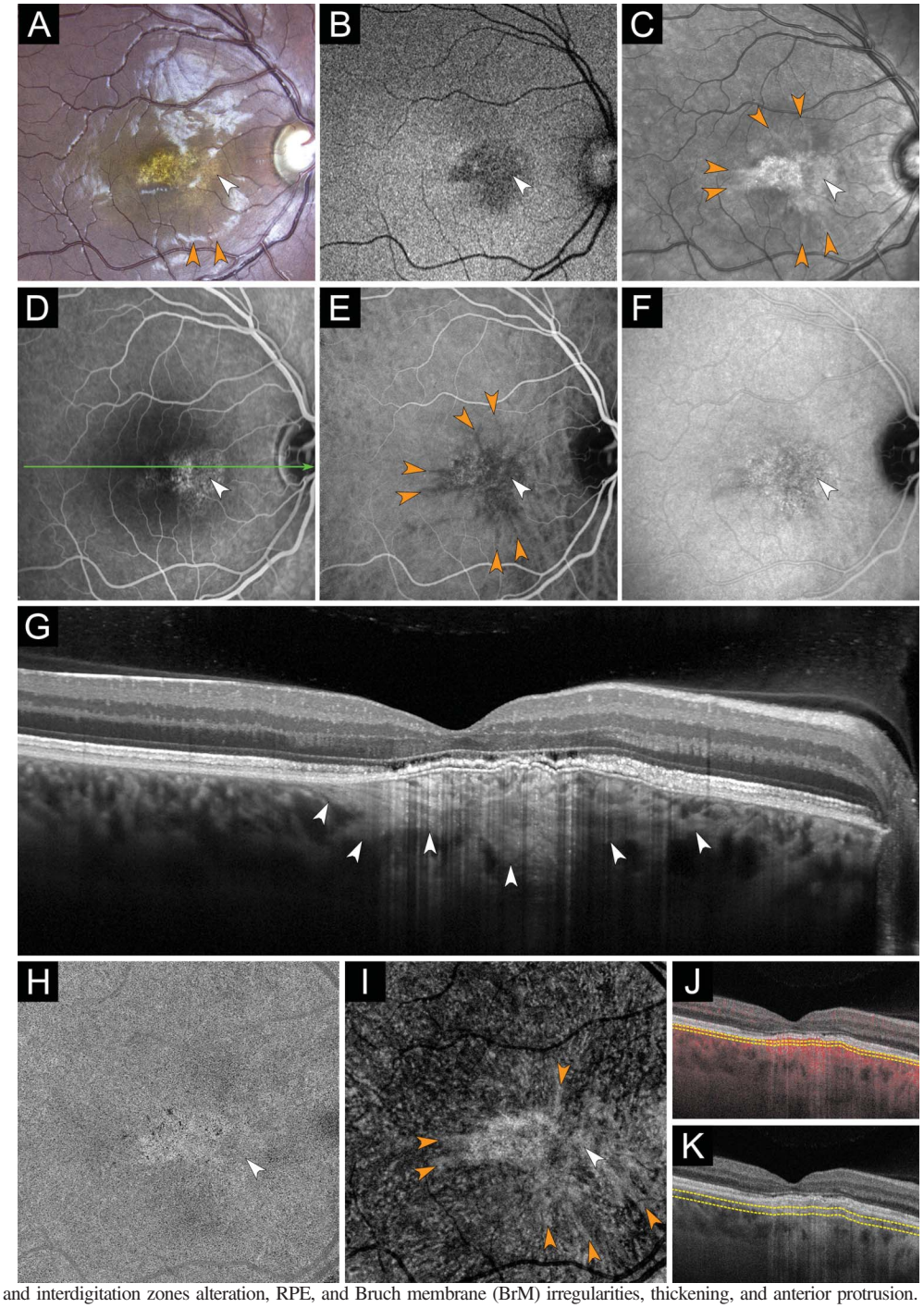

Fig. 2. Multimodal imaging and high-resolution optical coherence tomography of SMACH (Case 2). Patient diagnosed with chronic central serous chorioretinopathy at the age of 17 years. **A.** Confocal color fundus photography of the right eye shows a subfoveal yellowish orange choroidal lesion (*white arrowhead*) with subtle orange finger-like extensions inferiorly (*orange arrowheads*). Note the fine pigment stippling surrounded by hypopigmentary changes in the macula. **B.** Green-light fundus autofluorescence image shows hypoautofluorescence (*white arrowhead*) in the macula corresponding to areas of retinal pigment epithelium (RPE) disruption. **C.** On the near-infrared reflectance image, the lesion is hyperreflective (*white arrowhead*) with discrete hyperreflective finger-like extensions oriented radially in a stellate configuration (*orange arrowheads*). Overlying areas of RPE disruption exhibit speckled hyperreflectivity. **D.** Late phase of fluorescein angiography shows granular hypofluorescence and hyperfluorescence corresponding to RPE alterations (*white arrowhead*). The green line indicates the location of the high-resolution optical coherence tomography (OCT) B-scan in (**G**). **E.** Early phase of indocyanine green angiography (ICGA) shows hypofluorescence of the choroidal lesion (*white arrowhead*). Note the distinctive hypofluorescent finger-like projections arranged in a stellate configuration (*orange arrowheads*). **F.** Late phase of ICGA shows mild hypofluorescence (*white arrowhead*) co-localizing with the choroidal lesion and overlying RPE disruption (reduced RPE uptake). Note the absence of choroidal vascular hyperpermeability that could be typical of diseases that are part of the pachychoroid disease spectrum. **G.** High-resolution OCT B-scan through the fovea shows ellipsoid and interdigitation zones alteration, RPE, and Bruch membrane (BrM) irregularities, thickening, and anterior protrusion. Note the hyperreflective fibrous-like appearance characteristic of the choroidopathy (*white arrowheads*). There are no pachyvessels in the Haller layer compressing the inner choroid. The choroidal–scleral junction is visible. Posterior hypertransmission because of overlying RPE/BrM disruption is noted. **H.** En face OCTA segmented at the level of the choriocapillaris shows very subtle flow signal deficits co-localizing with the choroidal lesion (*white arrowhead*). **I.** En face structural OCT segmented at the level of the choroidal lesion shows hyperreflective changes (*white arrowhead*) with distinctive hyperreflective finger-like projections oriented radially in a stellate configuration (*orange arrowheads*). **J.** Cross-sectional OCTA with flow signal overlay. The yellow lines indicate the segmentation used to obtain the image in (**H**). **K.** Cross-sectional OCT, with the yellow lines indicating the segmentation used to obtain the image in (**I**).

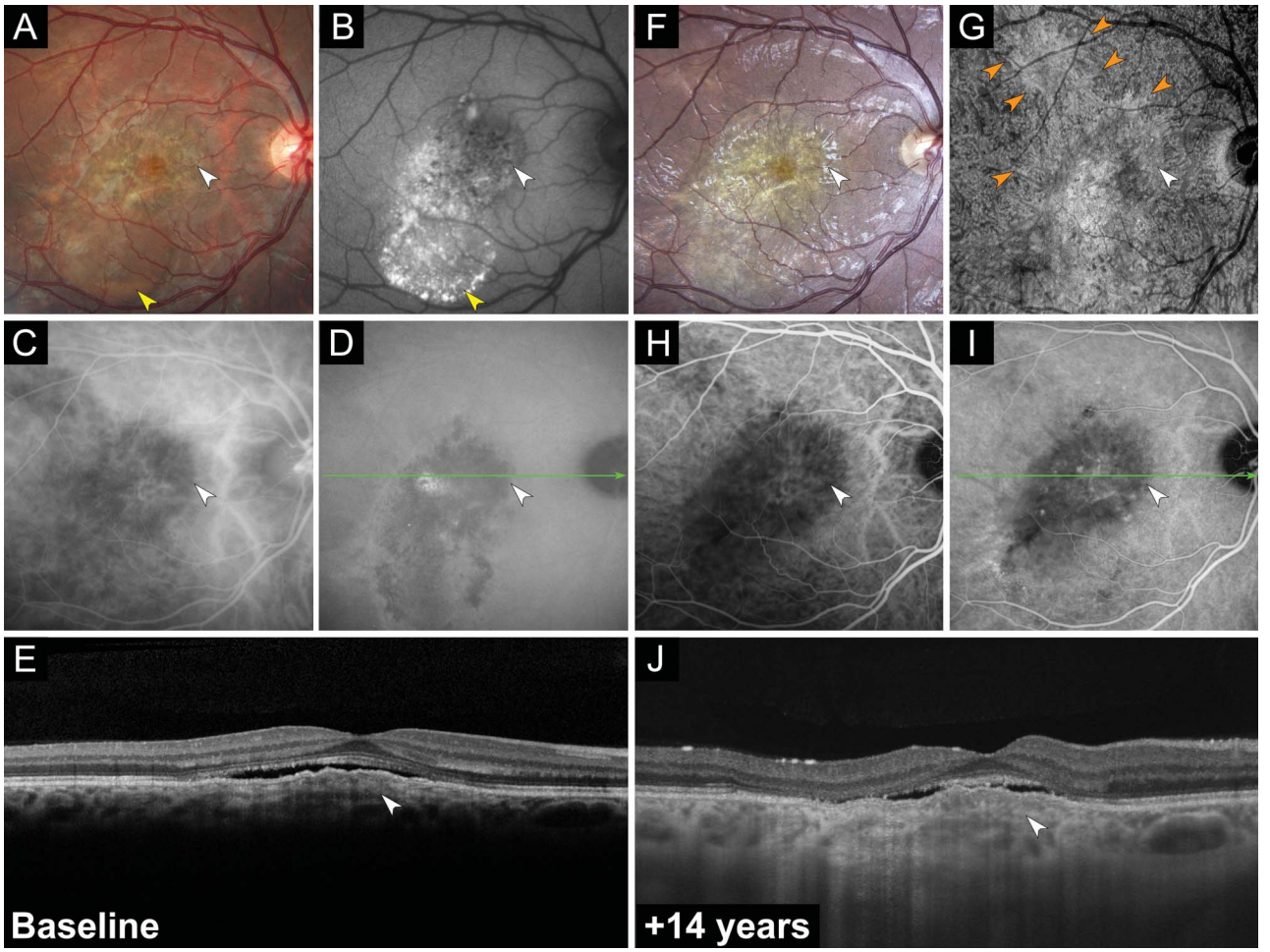

Fig. 3. Multimodal imaging of SMACH associated with an acquired vitelliform lesion and long-term follow-up images (Case 1). Patient diagnosed with chronic central serous chorioretinopathy at the age of 13 years. **A–E.** Baseline multimodal imaging performed at the age of 13 years. **A.** Color fundus photography of the right eye shows a yellowish choroidal lesion (*white arrowhead*) underlying pigmentary changes. Note the subretinal acquired vitelliform lesion gravitating inferiorly (*yellow arrowhead*). **B.** Blue-light fundus autofluorescence image shows speckled areas of hypoautofluorescence and hyperautofluorescence (*white arrowhead*) co-localizing with the choroidal lesion. Note the hyperautofluorescence inferiorly corresponding to the vitelliform material deposition (*yellow arrowhead*). **C.** Early phase of indocyanine green angiography (ICGA) shows filling delay and hypofluorescence of the choroidal lesion (*white arrowhead*). **D.** Late phase of ICGA shows hypofluorescence (*white arrowhead*) co-localizing with the choroidal lesion and overlying retinal pigment epithelium (RPE) disruption (reduced RPE uptake). The green line indicates the location of the optical coherence tomography (OCT) B-scan in (**E**). **E.** Spectral-domain OCT B-scan through the fovea shows subretinal fluid and anterior protrusion of the RPE overlying a hyperreflective fibrous-like lesion of the inner choroid (*white arrowhead*). **F–J.** Fourteen-year follow-up multimodal imaging performed at the age of 27 years. **F.** Confocal color fundus photography shows a relative stability of the size of the choroidal lesion (*white arrowhead*). Note the regression of the acquired vitelliform lesion inferiorly. **G.** En face structural OCT segmented at the level of the choroidal lesion shows hyperreflective changes (*white arrowhead*) with distinctive finger-like projections (*orange arrowheads*). The extent of the choroidal lesion on en face structural OCT exceeds the one assessed on ophthalmoscopy. **H.** Early phase of ICGA shows filling delay and hypofluorescence of the choroidal lesion (*white arrowhead*). Note the relative stability of the early-phase ICGA findings during follow-up. **I.** Late phase of ICGA shows hypofluorescence (*white arrowhead*) co-localizing with the choroidal lesion and overlying RPE disruption (reduced RPE uptake). Note the relative stability of the late-phase ICGA findings during the follow-up. There is no choroidal vascular hyperpermeability. The green line indicates the location of the OCT B-scan in (**J**). **J.** Swept source OCT B-scan through the fovea shows persistent subretinal fluid with disruption of the ellipsoid and interdigitation zones. The choroid is structurally altered with thickening and hyperreflectivity of the inner choroidal stroma (*white arrowhead*). There are no pachyvessels, and the choroidal–scleral junction is visible. Note the relative stability of the anterior protrusion of the RPE induced by the choroidal lesion during the follow-up.

Ophthalmoscopic Features

On funduscopic examination, all patients presented with an unilateral, yellowish orange, dendriform, choroidal lesion underlying nonspecific hypopigmentary and hyperpigmentary changes of the RPE. The choroidal lesion was located under the fovea in 12 eyes (67%), in the parafovea in five eyes (28%), and in the nasal retina in one eye (5%). The shape and size of the choroidal lesion were variable, but distinctive finger-like extensions pointing radially in a stellate configuration were seen in all cases. Subretinal fluid accumulation was observed in 10 eyes (56%) and an

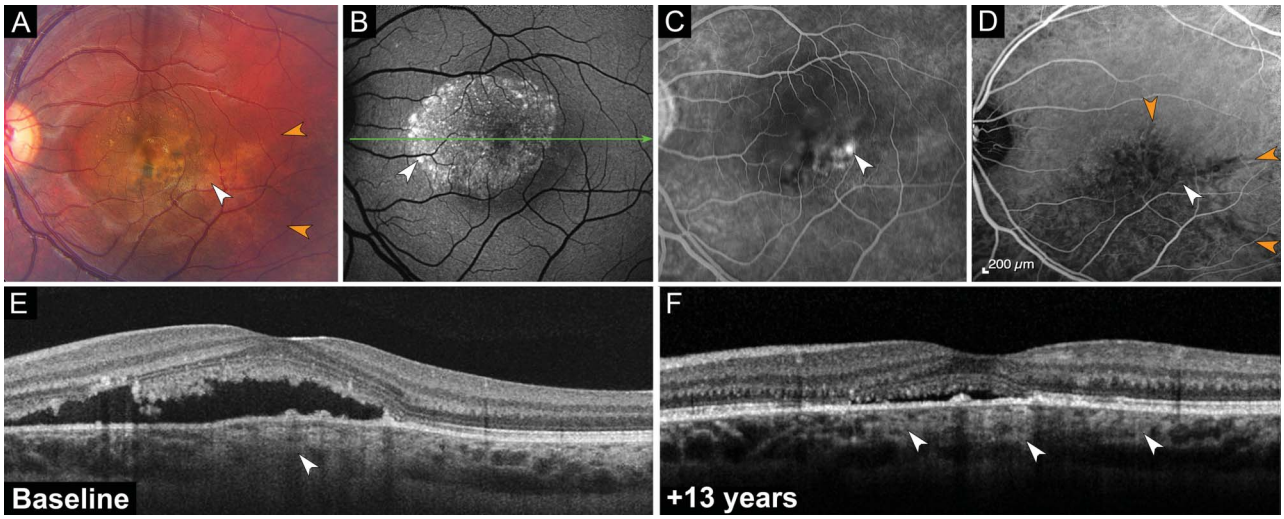

Fig. 4. Multimodal imaging of SMACH masquerading as best vitelliform macular dystrophy and long-term follow-up images (Case 6). Patient with a presumed diagnosis of unilateral best vitelliform macular dystrophy at the age of 7 years. **A**–**E.** Baseline multimodal imaging performed at the age of 7 years. **A.** Color fundus photography of the left eye shows a yellowish orange choroidal lesion (*white arrowhead*). Note the distinctive finger-like projections pointing toward the temporal periphery (*orange arrowheads*). Subretinal fluid is apparent with vitelliform material deposition and areas of retinal pigment epithelium (RPE) hyperpigmentation. **B.** Blue-light fundus autofluorescence image shows speckled hypoautofluorescence in the fovea surrounded by a rim of hyperautofluorescence (*white arrowhead*). The green line indicates the location of the optical coherence tomography (OCT) B-scan in (**E**). **C.** Late phase of fluorescein angiography shows focal RPE leakage (*white arrowhead*) and blockage from mottled RPE hyperpigmentation. **D.** Late phase of indocyanine green angiography shows hypofluorescence (*white arrowhead*) co-localizing with the choroidal lesion and overlying RPE disruption (reduced RPE uptake). Note the distinctive hypofluorescent finger-like projections oriented radially (*orange arrowheads*). There is no choroidal vascular hyperpermeability. **E.** Spectral-domain OCT B-scan through the fovea shows subretinal fluid and mild anterior protrusion of the RPE by a hyperreflective fibrous-like lesion of the choroid (*white arrowhead*). **F.** Follow-up spectral-domain OCT B-scan performed at the age of 20 years. Note the persistent subretinal fluid overlying RPE alteration. The choroidal lesion is hyperreflective and located in the inner choroid (*white arrowheads*).

acquired vitelliform lesion was seen in two eyes (11%). No cases showed evidence of active intraocular inflammation.

Multimodal Imaging Features

On cross-sectional OCT, the choroidal lesion showed hyperreflective fibrous-like changes in the inner choroid in all cases. The mean thickness of the choroidal lesion was 125 ± 90 μm (range, 52–315 μm). The choroidal lesion displayed no optical shadowing; posterior hypertransmission was noted in eyes with overlying disruption of the RPE/Bruch membrane (BrM) complex. The normal outer choroidal vasculature beneath the choroidal lesion and the choroidal–scleral junction were visible in all cases. No cases showed dilation of the choroidal vessels in the Haller layer (*pachyvessels*) compressing the inner choroid and choriocapillaris.

Adjunctive outer retinal damages included irregularities, thickening, and anterior protrusion of the RPE/BrM complex (100%), subtle ellipsoid zone (EZ) and interdigitation zone (IZ) attenuation (61%), complete EZ/IZ loss resembling outer retinal cavitation (11%), external limiting membrane alteration (22%), outer nuclear layer thinning (44%), and SRF (56%). An outward protrusion of the posterior curvature of the RPE/BrM complex adjacent to the choroidal lesion and resembling a focal staphyloma was seen in two eyes (11%).

On OCTA, subtle flow signal deficits at the level of the choriocapillaris co-localized with the choroidal lesion. No cases showed evidence of MNV. En face structural OCT segmented at the level of the choroidal lesion showed hyperreflective changes with distinctive hyperreflective finger-like projections oriented radially in a stellate configuration.

On NIR, the choroidal lesion was hyperreflective and more apparent in the absence of overlying SRF. Hyperreflective finger-like projections oriented radially were seen in all cases. Focal hyperreflectivity corresponding to hyperpigmentation of the RPE was also observed.

On FAF, six eyes (33%) showed no alterations, seven eyes (39%) showed speckled hypoautofluorescence associated with disruption of the photoreceptor and RPE layers, and three eyes (17%) showed a hyperautofluorescent rim associated with acquired vitelliform lesions and SRF.

FA showed granular hypofluorescence and hyperfluorescence corresponding to mottled RPE alterations in all cases. Late focal staining and focal leakage were seen in 7 (39%) and 3 cases (17%), respectively. ICGA showed

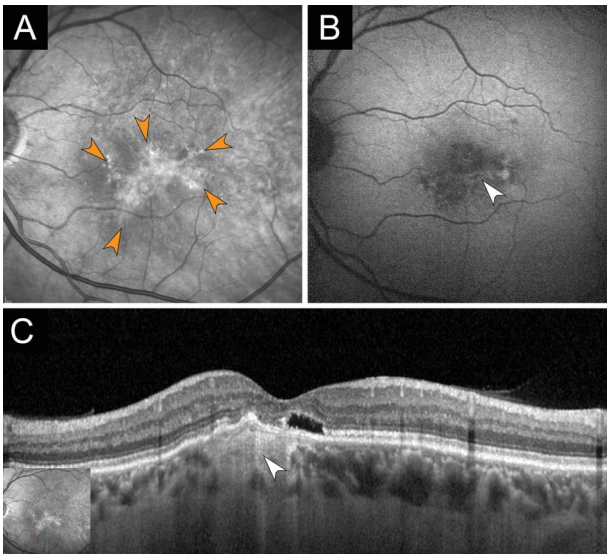

Fig. 5. Multimodal imaging of SMACH associated with foveal optical gap on optical coherence tomography (Case 3). Patient diagnosed with chronic central serous chorioretinopathy at the age of 20 years. **A.** Near-infrared reflectance image of the left eye shows a hyperreflective lesion with typical hyperreflective finger-like projections (*orange arrowheads*) arranged in a stellate configuration. **B.** Blue-light fundus autofluorescence image shows speckled hyperautofluorescence (*white arrowhead*) co-localizing with retinal pigment epithelium (RPE) mottling. **C.** Spectral-domain optical coherence tomography (OCT) B-scan through the fovea shows a hyperreflective fibrous-like choroidal lesion located in the inner choroid (*white arrowhead*), resulting in anterior protrusion and alteration of the RPE. Note the focal interruption of the ellipsoid and interdigitation zones in the fovea resembling outer retinal cavitation or "optical gap." There are no dilated outer choroidal vessels in the Haller layer (pachyvessels). The normal outer choroidal vasculature beneath the choroidal lesion is attenuated but still visible, and the choroidal–scleral junction is apparent. The inset is the near-infrared reflectance image, with the green line indicating the location of the OCT B-scan.

delayed filling with early phase and late-phase hypofluorescence. The distinctive finger-like projections were hypofluorescent. There was no observable disparity in both the extent and the degree of hypofluorescence on ICGA between the cases with and without SRF. No cases showed MNV or focal choroidal hyperpermeability on mid-to-late-phase ICGA. Figures 1–7 illustrate the multimodal imaging findings of SMACH.

ERG, EOG, and Microperimetry Features

Full-field ERG and EOG were performed in 4 cases and were normal. Retinal sensitivity on microperimetry over the choroidal lesion was assessed in one eye and showed a mild decrease compared with adjacent areas of normal retina.

Evolution of SMACH over Time

During the follow-up period, the size and shape of the choroidal lesion remained stable in all cases. During a mean follow-up of 6 years (range, 2–19 years), eight patients (44%) showed no evidence of SRF or resolved SRF on OCT and FAF imaging, respectively (Figure 1). Seven patients (39%) showed spontaneous fluctuations of SRF volume on OCT (Figures 3 and 4). None of the cases developed MNV. Treatments including PDT (4 eyes, 22%) and intravitreal anti-VEGF injections (3 eyes, 17%) showed no effect on SRF.

Discussion

In this report, we describe characteristic clinical and imaging features of a series of 18 cases of SMACH which, to our knowledge, includes all known cases to date (15 unpublished cases and three previously reported).[1] Clinically, SMACH is characterized by a yellowish orange multiform choroidal lesion. Distinctive OCT features include hyperreflective fibrous-like changes located in the inner choroidal stroma, resulting in anterior protrusion of the RPE/BrM and outer retinal alterations. Typical finger-like projections arranged in a stellate configuration are best seen on NIR, ICGA, and en face OCT imaging and should be considered in making the diagnosis. OCTA shows minimal alteration of the choriocapillaris overlying the choroidal lesion. Adjunctive imaging modalities, including FAF and FA, show nonspecific changes related to outer retinal and RPE disruption. Long-term follow-up shows stability of the choroidal lesion. Visual acuity was overall preserved, although three eyes had BCVA <20/40 and one patient had marked progressive visual impairment (from 20/20 to 20/200 after 14 years of follow-up). SRF accumulation shows spontaneous fluctuations in volume and has been found to be unresponsive to treatment (i.e., PDT and intravitreal anti-VEGF injections). Absence of SRF in eight patients (44%) with no visual symptoms may suggest a preclinical asymptomatic stage of SMACH. Nonetheless, one patient followed for 19 years did not develop serous retinal detachment (Case 12). Therefore, "Serous Maculopathy due to Aspecific CHoroidopathy" may be more appropriately referred to as "Stellate Multiform Amelanotic CHoroidopathy." This change in nomenclature allows for keeping the original acronym SMACH proposed by Van Dijk and Boon.[1]

Patients' demographic and clinical characteristics showed that SMACH may be associated with vision loss related to SRF accumulation and outer retinal disruption predominantly in young patients. Therefore, SMACH may masquerade as chorioretinal conditions typically seen in patients in their 20s to 40s, including early-onset CSC,[3–5] inherited retinal diseases, inflammatory chorioretinopathies, and choroidal tumors.

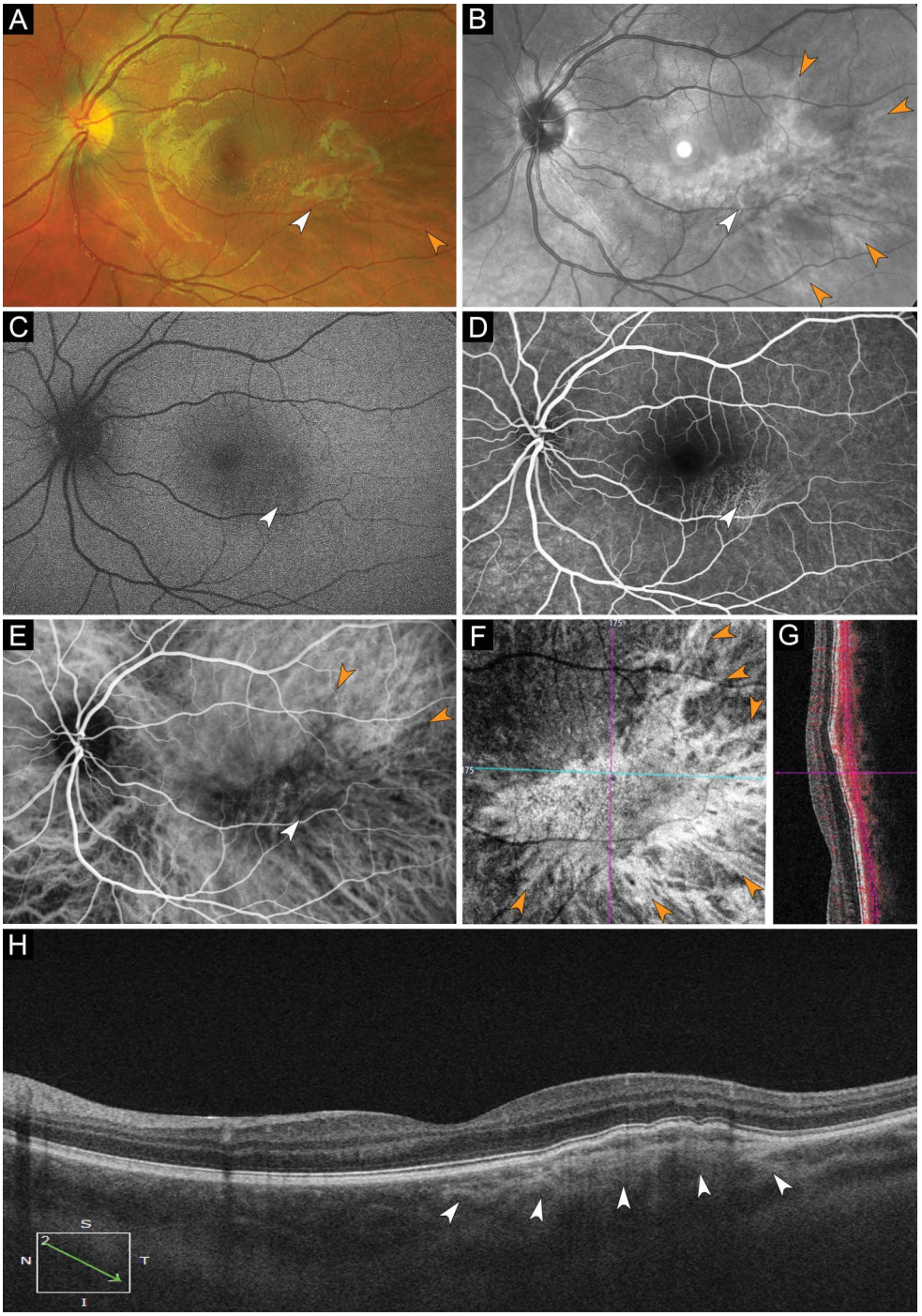

Fig. 6. Multimodal imaging of a large asymptomatic SMACH (Case 5). Patient diagnosed with placoid chorioretinitis at the age of 15 years. **A.** Pseudocolor fundus photography of the left eye shows a parafoveal, yellowish orange, dendriform, choroidal lesion (*white arrowhead*) with subtle orange finger-like extension inferiorly (*orange arrowhead*). Note the fine pigment stippling inferotemporal to the fovea. **B.** On near-infrared reflectance image, the lesion is hyperreflective (*white arrowhead*) with distinctive hyperreflective finger-like extensions oriented radially in a stellate configuration (*orange arrowheads*). **C.** Green-light fundus autofluorescence image shows minimal hypoautofluorescent changes co-localizing with the choroidal lesion and pigmentary alterations (*white arrowhead*). **D.** Late phase of fluorescein angiography shows granular hypofluorescence and hyperfluorescence corresponding to retinal pigment epithelium (RPE) alterations (*white arrowhead*). **E.** Early phase of indocyanine green angiography shows hypofluorescence of the choroidal lesion (*white arrowhead*). Note the distinctive hypofluorescent finger-like projections arranged in a stellate configuration (*orange arrowheads*). **F.** En face structural optical coherence tomography (OCT) segmented at the level of the choroidal lesion shows hyperreflective changes with distinctive hyperreflective finger-like projections oriented radially in a stellate configuration (*orange arrowheads*). **G.** Cross-sectional OCT angiography, with the red lines indicating the segmentation used to obtain the image in (**F**). **H.** Swept-source OCT B-scan through the fovea shows anterior protrusion of the RPE by a hyperreflective fibrous-like lesion of the inner choroid (*white arrowheads*). There are no pachyvessels in the Haller layer compressing the inner choroid. The choroidal–scleral junction and the normal outer choroidal vasculature beneath the choroidopathy are visible. Note the relative preservation of the ellipsoid and interdigitation zones and the absence of subretinal fluid. The green line indicates the location of the OCT B-scan.

Especially, detection of the choroidal lesion on ophthalmoscopic examination may be hindered by overlying SRF and pigmentary changes. Nonetheless, imaging and diagnostic testing were not consistent with any of these diseases. None of the eyes with SMACH presented with features suggestive of pachychoroid disease spectrum, including pachyvessels compressing the inner choroid on cross-sectional OCT or focal choroidal hyperpermeability on mid-to-late-phase ICGA, thereby excluding CSC.[6,7] Moreover, we observed a focal increase in choroidal thickness on OCT related to the choroidal lesion rather than

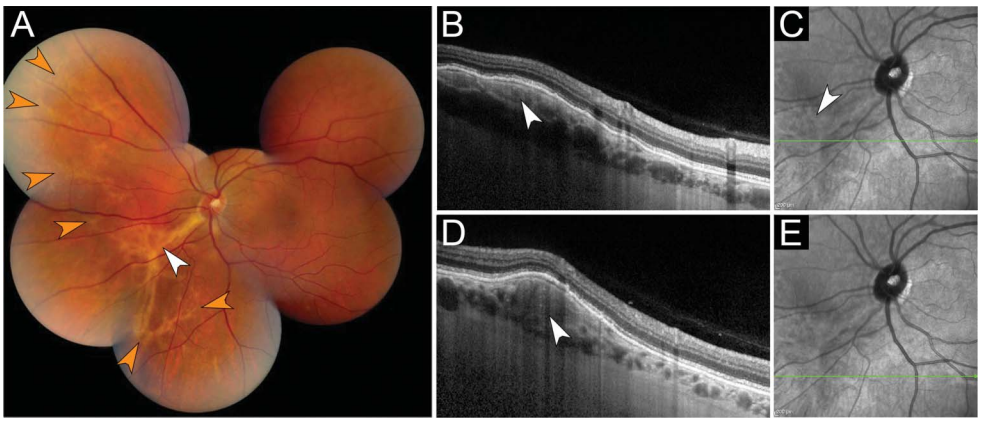

Fig. 7. Multimodal imaging of extramacular SMACH (Case 15). Patient diagnosed with unspecified choroidal tumor at the age of 51 years. **A.** Montage of color fundus photographs of the left eye shows a large yellowish orange choroidal lesion (*white arrowhead*) in the nasal retina and sparing the macula. Note the distinctive finger-like projections pointing toward the nasal periphery (*orange arrowheads*). **B.** Spectral-domain optical coherence tomography (OCT) B-scan shows a hyperreflective fibrous-like choroidal lesion located in the inner choroid (*white arrowhead*). Note the focal attenuation of the overlying ellipsoid zone and interdigitation zone. There are no dilated outer choroidal vessels in the Haller layer (pachyvessels). The normal outer choroidal vasculature beneath the choroidal lesion is attenuated but still visible, and the choroidal–scleral junction is apparent. **C.** Near-infrared reflectance image of the left eye shows a hyperreflective lesion in the nasal retina (*white arrowhead*). The green line indicates the location of the OCT B-scan displayed in (**B**). **D.** Spectral-domain OCT B-scan shows a hyperreflective fibrous-like choroidal lesion. Note the prominent anterior protrusion and alteration of the retinal pigment epithelium (*white arrowhead*). **E.** Near-infrared reflectance image of the left eye shows a hyperreflective lesion in the nasal retina. The green line indicates the location of the OCT B-scan displayed in (**D**).

congestion of the choroidal vasculature as seen in CSC.[6,7] This finding was supported by our imaging analysis showing subtle flow signal deficits of the choriocapillaris on OCTA and a choroidal filling delay with mild late hypofluorescence on ICGA. SMACH may also be misinterpreted as inflammatory placoid chorioretinitis. However, none of the cases showed intraocular inflammation or expansion of the choroidal lesion over time. Placoid chorioretinitis typically shows hyporeflectivity and loss of the normal inner choroidal architecture on OCT, massive choriocapillaris flow signal deficits on OCTA, and intense hypofluorescence on early phase and late-phase ICGA.[8] Alternatively, inherited retinal diseases were also considered in view of the early detection of the retinal changes, the presence of outer retinal cavitation on OCT, and hyperautofluorescent changes on FAF. Foveal cavitation or "optical gap" on OCT is a distinctive finding of cone dystrophy, including achromatopsia, *ABCA4*-related retinopathy, and occult macular dystrophy.[9–11] Similarly, hyperautofluorescent rims and vitelliform material gravitating inferiorly have been reported in Best vitelliform macular dystrophy.[12] However, our cases were strictly unilateral and nonprogressive, and no patients had a positive family history for inherited retinal disease. As further confirmation, available genetic testing found no pathogenic mutations, and full-field ERG and EOG performed in selected cases were not suggestive of panretinal photoreceptor or RPE dysfunction. Finally, the clinical course and multimodal imaging features of SMACH lacked the defining findings of other reported choroidal and scleral lesions, including amelanotic choroidal nevus and melanoma, choroidal osteoma, choroidal metastasis, circumscribed choroidal hemangioma, choroidal lymphoma, or focal scleral nodule.[13,14] Table 2 summarizes the characteristic multimodal imaging features of SMACH and its differential diagnoses.[13–28]

The pathogenesis of SMACH is unclear. The early onset of detection (youngest patient: 7 years old) and relative stability of the lesion size may suggest a congenital dysgenesis of the choroid. Progressive alteration of the choriocapillaris and RPE by the choroidal lesion may be the cause of SRF accumulation. The mechanisms of SRF accumulation may parallel those of choroidal naevi, where a mass effect on the choriocapillaris results in increased intravascular hydrostatic pressure and fluid transudation.[28] Focal RPE leakage, as seen in three eyes (17%), can be interpreted as damage to the outer blood–retinal barrier, which may also promote SRF accumulation.[28] The staphyloma-like changes adjacent to the choroidal lesion seen in two eyes (11%) may result in abnormal choroidal blood flow, RPE dysfunction, and subsequent SRF accumulation.[29] Importantly, 8 cases (44%) with minimal alterations of the outer retina showed no evidence of SRF, suggesting that alterations of the retinal and choroidal structures must reach a critical threshold for SRF accumulation. In the absence of clinicopathologic correlation, the nature of this choroidopathy remains elusive. Nonetheless, it may represent a variant of more common amelanotic choroidal tumors, including choroidal nevus. An amelanotic choroidal nevus is commonly distinguished by the presence of a yellowish, ill-defined, round-shaped choroidal lesion, which may exhibit overlying drusen, pigment clumps and a halo of

Table 2. Characteristic Multimodal Imaging Features of SMACH and Differential Diagnoses

Etiology Multimodal Imaging	SMACH	Amelanotic Choroidal Nevus[13,15–18,28]	Amelanotic Choroidal Melanoma[13,15,17–19]	Choroidal Osteoma[13,20,21]
Color fundus photography	Yellowish orange dendriform choroidal lesion (100%) Subretinal fluid (59%), acquired vitelliform lesion (12%)	Yellowish, ill-defined, round-shaped choroidal lesion Possible overlying drusen, pigment clumps, and halo of depigmentation	Elevated yellowish choroidal mass with subretinal fluid, orange pigment, and absence of drusen	Yellow–orange calcified plaque with sharp margins
Optical coherence tomography	Hyperreflective fibrous-like changes of the inner choroid (100%) Anterior protrusion of the RPE (100%) Subretinal fluid (59%)	Gently domed smooth-surfaced choroidal mass Choriocapillaris thinning Posterior optical shadowing	Elevated choroidal lesion with subretinal fluid, shaggy photoreceptors, and disruption of the overlying retina Choriocapillaris compression Posterior optical shadowing	Flat, dome, or undulating choroidal mass with hyperreflective horizontal lines (bone lamella and cement line), hyporeflective horizontal and vertical tubules (vascular channels) and speckled appearance (spongy trabecular or compact bone)
En face optical coherence tomography	Hyperreflective lesion (100%) Hyperreflective finger-like projections oriented radially (100%)	Hyperreflective lesion repelling the normal choroidal vasculature	Hyperreflective lesion repelling the normal choroidal vasculature	Variable reflectivity
Fundus autofluorescence	Nonspecific speckled hyperautofluorescence (41%) Normal (35%)	Normal or nonspecific stippled hypoautofluorescent and hyperautofluorescent changes	Confluent hyperautofluorescence with hypoautofluorescent lacunae	Normal or nonspecific stippled hypoautofluorescent and hyperautofluorescent changes
Near-infrared reflectance	Hyperreflective lesion (100%) Hyperreflective finger-like projections oriented radially (100%)	Hyperreflective round-shaped lesion	Hyperreflective lesion	Hyperreflective lesion
Fluorescein angiography	Nonspecific granular hypofluorescence and hyperfluorescence (100%)	Nonspecific granular hypofluorescence and hyperfluorescence	Early blockage and late hyperfluorescent spots	Early patchy hyperfluorescence and late diffuse staining
Indocyanine green angiography	Early and late hypofluorescence (100%) Hypofluorescent finger-like projections oriented radially (100%) No choroidal vascular hyperpermeability (100%)	Early and late hypofluorescence	"Double circulation" pattern	Early and late hypofluorescence
Optical coherence tomography angiography	Subtle flow signal deficits of the choriocapillaris (100%) No evidence of choroidal neovascularization (100%)	Decrease flow signal of the choriocapillaris	Intralesional vascularity Compression of the choriocapillaris and choroid	Fine vascular network within the tumor
Natural course and complications	Nonprogressive Spontaneous fluctuations of the subretinal fluid	Possible growth and melanoma transformation Choroidal nevus-associated subretinal fluid and choroidal neovascularization	Tumor growth Retinal detachment Systemic metastasis	Tumor growth Choroidal neovascularization, subretinal fluid, and outer retinal atrophy

Table 2. (*Continued*)

Etiology Multimodal Imaging	Choroidal Metastasis[13,22]	Circumscribed Choroidal Hemangioma[13,23–25]	Choroidal Lymphoma[13,26,27]	Focal Scleral Nodule[14]
Color fundus photography	Soft yellow choroidal mass with subretinal fluid	Reddish orange, round-to-oval choroidal lesion	Yellow patchy choroidal infiltration	Yellowish white round-shaped scleral lesion with an orange halo ("helioid appearance")
Optical coherence tomography	Elevated hyporeflective choroidal lesion with an irregular surface ("lumpy bumpy" appearance) and disruption of the overlying retina	Elevated hyporeflective choroidal lesion with smooth, gently sloping surface	Hyporeflective choroidal thickening with different surface appearance (placid, rippled, seasick)	Intrascleral lesion with a dome-shaped, nodular or volcanic configuration
	Choriocapillaris compression	Intralesional expansion of choroidal vessels without compression of the choriocapillaris	Inward compression of the choroid	Compression of the overlying choriocapillaris and choroid
	Posterior optical shadowing	Disruption of the overlying retina, subretinal and intraretinal fluid		Disruption of the overlying retina and subretinal fluid
En face optical coherence tomography	Hyporeflective lesion	Hyporeflective multilobular pattern	Hyporeflective infiltration	Hyporeflective lesion
Fundus autofluorescence	Nonspecific hypoautofluorescent and hyperautofluorescent changes	Nonspecific hypoautofluorescent and hyperautofluorescent changes	Hypoautofluorescent and hyperautofluorescent spots ("leopard spots" or "giraffe skin" pattern)	Hypoautofluorescent and hyperautofluorescent changes
Near-infrared reflectance	Hyporeflective lesion	Hyporeflective lesion	Hyporeflective and hyperreflective changes	Hyperreflective lesion
Fluorescein angiography	Early blockage and late staining with pinpoint leakage	Early hyperfluorescence and late staining	Hypofluorescent and hyperfluorescent spots (inverted pattern compared with fundus autofluorescence)	Early hyperfluorescence and late staining
Indocyanine green angiography	Early hypofluorescence and late patchy staining	Early filling of the lesion, intense mid-phase hyperfluorescence, and late central hypofluorescence ("wash-out")	Early and late hypofluorescence	Early and late hypofluorescence
Optical coherence tomography angiography	Absence of intrinsic vascularity Compression of the choriocapillaris and choroid	Intrinsic vascularity ("bag of worms" and "spaghetti-like" patterns)	Compression of the choriocapillaris and choroid	Absence of intrinsic vascularity Compression of the choriocapillaris and choroid
Natural course and complications	Tumor growth and invasion	Choroidal neovascularization, subretinal fluid, intraretinal fluid, and outer retinal atrophy	Tumor growth and invasion Subretinal fluid and outer retinal atrophy	Poorly progressive (possible growth and spontaneous regression) Subretinal fluid and outer retinal atrophy

depigmentation.[13] Cross-sectional OCT typically demonstrates a smoothly contoured, dome-shaped choroidal mass with posterior shadowing, and OCTA exhibits alteration of the choriocapillaris.[15,28] Although amelanotic choroidal naevi may present with hyperreflective characteristics on NIR, the presence of hyperreflective, radially oriented finger-like projections has not, to our knowledge, been reported.[16]

Appropriate therapeutic management cannot be provided owing to the limited number of cases reported. None of our cases demonstrated positive responses to therapeutic interventions, including PDT and intravitreal anti-VEGF injections. Moreover, spontaneous fluctuation of the SRF was noted in some untreated cases. Our long-term follow-up findings suggest that this choroidopathy is not progressive. Long-term visual prognosis may be influenced by the amount of central outer retinal alterations that can increase over time in some patients. Additional treatments may be required for specific complications,

including MNV, although this complication was not observed in this cohort.

Limitations of this study include the relatively few patients, the retrospective nature, and the lack of complete multimodal imaging evaluation in some cases. However, SMACH is a very recently described entity, and we believe our study may help identify other cases.

In conclusion, we expand the description of a recently reported clinical entity abbreviated "SMACH" and propose revised nomenclature (Stellate Multiform Amelanotic CHoroidopathy) that more precisely fits its clinical spectrum, including an absence of SRF in 44% of known cases. SMACH is characterized by a unique imaging pattern lacking the defining features of other known choroidal lesions. Patients with SMACH may present with early-onset vision loss related to SRF accumulation and foveal outer retinal disruption. SMACH may masquerade as other early-onset macular diseases, including CSC, inherited retinal diseases, inflammatory chorioretinitis, and choroidal tumors. Eyes with SMACH can be identified noninvasively based on a combination of multimodal imaging modalities, especially NIR, cross-sectional and en face OCT. Angiographic evaluation may further aid in establishing the diagnosis of this rare clinical picture. A high index of suspicion is required to recognize SMACH and avoid unnecessary investigations and inappropriate treatments.

Key words: multimodal imaging, optical coherence tomography, SMACH, stellate multiform amelanotic choroidopathy.

References

1. van Dijk EHC, Boon CJF. Serous business: delineating the broad spectrum of diseases with subretinal fluid in the macula. Prog Retin Eye Res 2021;84:100955.
2. van Dijk EHC, Ossewaarde-van Norel J, Vingerling JR, et al. Serous maculopathy due to aspecific choroidopathy (SMACH). Asia Pac J Ophthalmol 2022. Publish Ahead of Print.
3. Fine SL, Owens SL. Central serous retinopathy in a 7-year-old girl. Am J Ophthalmol 1980;90:871–873.
4. Kim YC, Kim SD, Kim KS. A case of idiopathic central serous chorioretinopathy in a 12-year-old male treated with bevacizumab. Korean J Ophthalmol 2012;26:391–393.
5. Velazquez-Martin JP, Fulda E, Domville D, et al. Presumed idiopathic central serous chorioretinopathy in a 12-year-old girl. Case Rep Ophthalmol 2012;3:5–10.
6. Cheung CMG, Lee WK, Koizumi H, et al. Pachychoroid disease. Eye (Lond). 2019;33:14–33.
7. Ramtohul P, Cabral D, Oh D, et al. En face ultra-widefield OCT of the vortex vein system in central serous chorioretinopathy. Ophthalmol Retina 2023;7:346–353.
8. Klufas MA, Phasukkijwatana N, Iafe NA, et al. Optical coherence tomography angiography reveals choriocapillaris flow reduction in placoid chorioretinitis. Ophthalmol Retina 2017;1:77–91.
9. Leng T, Marmor MF, Kellner U, et al. Foveal cavitation as an optical coherence tomography finding in central cone dysfunction. Retina 2012;32:1411–1419.
10. Greenberg JP, Sherman J, Zweifel SA, et al. Spectral-domain optical coherence tomography staging and autofluorescence imaging in achromatopsia. JAMA Ophthalmol 2014;132:437–445.
11. Oh JK, Ryu J, Lima de Carvalho JR, et al. Optical gap biomarker in cone-dominant retinal dystrophy. Am J Ophthalmol 2020;218:40–53.
12. Zatreanu L, Freund KB, Leong BCS, et al. Serous macular detachment in best disease: a masquerade syndrome. Retina 2020;40:1456–1470.
13. Shields CL, Pellegrini M, Ferenczy SR, Shields JA. Enhanced depth imaging optical coherence tomography of intraocular tumors: from placid to seasick to rock and rolling topography—the 2013 Francesco Orzalesi Lecture. Retina 2014;34:1495–1512.
14. Fung AT, Waldstein SM, Gal-Or O, et al. Focal scleral nodule: a New name for solitary idiopathic choroiditis and unifocal helioid choroiditis. Ophthalmology 2020;127:1567–1577.
15. Francis JH, Pang CE, Abramson DH, et al. Swept-source optical coherence tomography features of choroidal nevi. Am J Ophthalmol 2015;159:169–176.e1.
16. Jonna G, Daniels AB. Enhanced depth imaging OCT of ultrasonographically Flat choroidal nevi demonstrates 5 distinct patterns. Ophthalmol Retina 2019;3:270–277.
17. Shields CL, Dalvin LA, Ancona-Lezama D, et al. Choroidal nevus imaging features in 3,806 cases and risk factors for transformation into melanoma in 2,355 cases: the 2020 Taylor R. Smith and Victor T. Curtin Lecture. Retina 2019;39:1840–1851.
18. Greig EC, Laver NV, Mendonca LSM, et al. SWEPTSOURCE optical coherence tomography angiography in small choroidal melanomas and choroidal nevi. Retina 2021;41:1182–1192.
19. Shields CL, Bianciotto C, Pirondini C, et al. Autofluorescence of choroidal melanoma in 51 cases. Br J Ophthalmol 2008;92:617–622.
20. Olguin-Manríquez F, Enríquez AB, Crim N, et al. Multimodal imaging in choroidal osteoma. Int J Retina Vitreous 2018;4:30.
21. Shields CL, Arepalli S, Atalay HT, et al. Choroidal osteoma shows bone lamella and vascular channels on enhanced depth imaging optical coherence tomography in 15 eyes. Retina 2015;35:750–757.
22. Al-Dahmash SA, Shields CL, Kaliki S, et al. Enhanced depth imaging optical coherence tomography of choroidal metastasis in 14 eyes. Retina 2014;34:1588–1593.
23. Karimi S, Nourinia R, Mashayekhi A. Circumscribed choroidal hemangioma. J Ophthalmic Vis Res 2015;10:320–328.
24. Flores-Moreno I, Caminal JM, Arias-Barquet L, et al. En face mode of swept-source optical coherence tomography in circumscribed choroidal haemangioma. Br J Ophthalmol 2016;100:360–364.
25. Ramasubramanian A, Shields CL, Harmon SA, Shields JA. Autofluorescence of choroidal hemangioma in 34 consecutive eyes. Retina 2010;30:16–22.
26. Shields CL, Arepalli S, Pellegrini M, et al. Choroidal lymphoma shows calm, rippled, or undulating topography on enhanced depth imaging optical coherence tomography in 14 eyes. Retina 2014;34:1347–1353.
27. Mashayekhi A, Shukla SY, Shields JA, Shields CL. Choroidal lymphoma: clinical features and association with systemic lymphoma. Ophthalmology 2014;121:342–351.

28. Yu MD, Dalvin LA, Ancona-Lezama D, et al. Choriocapillaris compression correlates with choroidal nevus-associated subretinal fluid: OCT analysis of 3431 cases. Ophthalmology 2020; 127:1273–1276.

29. Cohen SY, Vignal-Clermont C, Trinh L, Ohno-Matsui K. Tilted disc syndrome (TDS): New hypotheses for posterior segment complications and their implications in other retinal diseases. Prog Retin Eye Res 2022;88:101020.